
7 Wetland InSAR

A Review of the Technique and Applications

Shimon Wdowinski and Sang-Hoon Hong

CONTENTS

Introduction.....	137
Synthetic Aperture Radar Observations.....	138
Wetland InSAR.....	140
Calibration and Validation.....	145
Interferometric Coherence of Wetlands.....	147
InSAR Time Series.....	147
Wetland InSAR Studies of Various Wetland Environments.....	149
Yellow River Delta Wetlands.....	149
Louisiana Wetlands.....	151
Sian Ka'an Biosphere Reserve.....	151
Danube Delta Wetlands.....	151
Discussion.....	151
Conclusion.....	152
Acknowledgments.....	153
References.....	153

INTRODUCTION

Wetlands are often very productive ecosystems, which can flourish due to water availability, nutrient cycling, and the sun's energy. They provide critical habitat for a wide variety of plant and animal species, including the larval stages of many ocean fish. Wetlands also deliver a wide range of important services, including water supply, water purification, carbon sequestration, coastal protection, and outdoor recreation (see Chapter 1). Globally, many such regions are under severe environmental stress, mainly from agriculture and urban developments, pollution, and rising sea level. However, there is an increasing recognition of the importance of these habitats, and mitigation and restoration activities have begun in a few regions. A key element in wetland conservation, management, and restoration involves hydrological monitoring as the entire ecosystem depends on its water supply. Heretofore, hydrological monitoring of wetlands is mostly conducted by stage (water level) measurements at gauging stations, which provides good temporal resolution but suffers from poor spatial resolution, as stage gauging stations are typically distributed several or even tens of kilometers from one another.

Remote sensing observations, in particular satellite imagery, serve as very useful tools for characterizing spatial phenomena, such as land cover and its changes over time. Optical and radar imageries have been widely used to detect and monitor wetlands, mainly for classifying vegetation and estimating biological parameters, like aboveground biomass (Evans and Costa 2013; Simard et al. 2006). Most of these remote sensing techniques cannot detect water level changes in wetlands, which occur beneath the vegetation cover. The one technique that is sensitive to water level

(i.e., height) changes in vegetated aquatic environments is wetland InSAR (interferometric synthetic aperture radar). This technique provides detailed maps of water level changes between two acquisition times and can be used to detect water level changes in various wetland environments (Wdowinski et al. 2004, 2008). The method has been successfully applied to study wetland hydrology in the Everglades (Hong et al. 2010a; Wdowinski et al. 2004, 2008), Louisiana (Kim et al. 2009; Kwoun and Lu 2009), and other locations (e.g., Gondwe et al. 2010).

This chapter provides a review of a wetland InSAR technique and applications, which are based on space-based synthetic aperture radar (SAR) observations. The first part of the chapter explains the differences between SAR and InSAR and provides technical information on available SAR data and satellites. The main part of the chapter focuses on the wetland InSAR technique, by presenting a brief physical explanation of the method, quality assessment of the results, and advanced InSAR time series methods for monitoring water level changes over time. The review ends with several examples where the method was applied for studying wetland hydrology around the globe and discusses future usage of the application.

SYNTHETIC APERTURE RADAR OBSERVATIONS

Space-based SAR is a very reliable technique for monitoring changes in both the terrestrial and aquatic surfaces of the Earth. SAR measures two independent observables, backscattered amplitude and phase, over a wide swath (10–400 km) with a pixel resolution of 1–100 m depending on the satellite acquisition parameters. Backscattered amplitude, which is often presented as gray-scale images of the surface (Figure 7.1b), is very sensitive to surface dielectric properties, surface

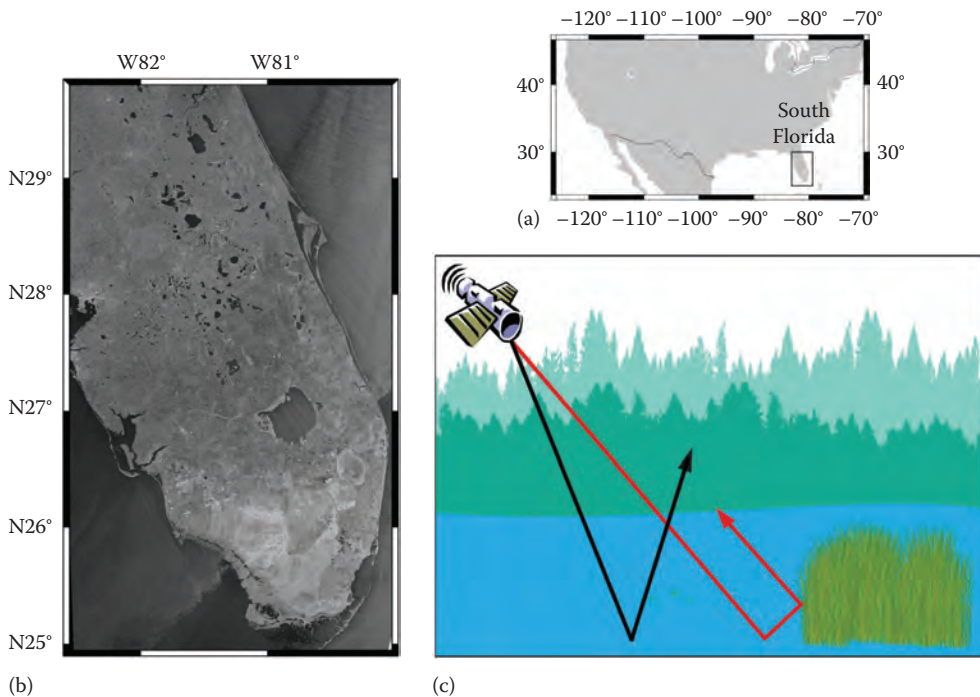


FIGURE 7.1 (a) Location map of our study area in south Florida. (b) Radarsat-1 ScanSAR image of study area (Radarsat data © Canadian Space Agency/Agence spatiale canadienne 2002. Processed by CStars and distributed by Radarsat International). (c) Cartoon illustrating the double-bounce radar signal return in vegetated aquatic environments. The red ray bounces twice and returns to the satellite, whereas the black ray bounces once and scattered away (specular reflectance).

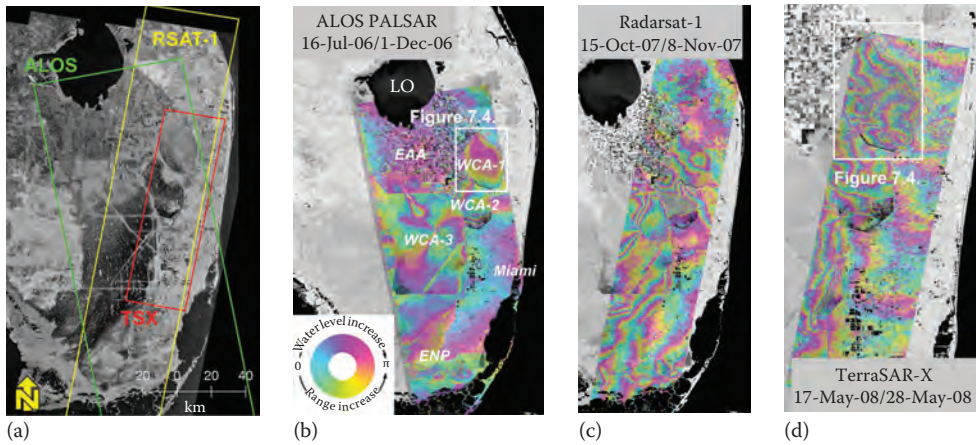


FIGURE 7.2 Interferograms showing phase changes, which were induced by water level changes in the Everglades wetlands, south Florida. (a) JERS-1 amplitude image of south Florida showing the location of the three interferograms. (b) L-band (24 cm wavelength) ALOS interferogram of 90 km wide ascending track. Each color cycle corresponds to 15 cm of water level change. (c) C-band (5.6 cm) Radarsat-1 interferogram of a 75 km wide descending swath. Each color cycle represents 4 cm of water level change. (d) X-band (3.1 cm) TSX interferogram of a 30 km wide descending swath. Some of the observed changes reflect changes in atmospheric moisture between the acquisitions. Each color cycle represents 2 cm of water level changes. LO, Lake Okeechobee; EAA, Everglades Agricultural Area; WCA, Water Conservation Area; ENP, Everglades National Park. The white boxes mark the location of a zoomed-in area shown in [Figure 7.4](#).

inclination toward the satellite, and wave direction in oceans (Bragg scattering). Amplitude images are widely used for studying land cover classification, soil moisture content, ocean waves, oil spill detection, and many other applications.

The second observable, backscattered phase measures the fraction of the radar wavelength that returns to the satellite's antenna. It is mainly sensitive to the range between the surface and the satellite but also to atmospheric conditions and changes in the surface dielectric properties. Phase data are mainly used in interferometric calculations (InSAR) for detecting centimeter-level displacements of the surface ([Figure 7.2](#)). The method compares pixel-by-pixel SAR phase observations of the same area acquired at different times from roughly the same location in space to produce high-spatial-resolution displacement maps. Such maps, termed interferograms ([Figure 7.2b](#) through [d](#)), are widely used in studies of earthquake-induced crustal deformation, magmatic activity (volcanoes), land subsidence due to water extraction, glacier movements, and more ([Wdowinski and Eriksson 2009](#)).

InSAR phase observations reflect distance changes in the line-of-sight (LOS) direction between the surface and the satellite. Because the SAR measurements are conducted in a slanted range geometry ([Figure 7.1b](#)), the LOS phase observations reflect a combined measure of both horizontal and vertical surface movements. When horizontal movements are negligible, the LOS phase signal can be translated to vertical surface movements, based on the radar half-wavelength and the acquisition geometry (vertical change = $\frac{\text{half-wavelength}}{\cos(\text{incidence angle})}$). We use the half-wavelength, because SAR satellites measure time differences between transmitted and received signals, which reflect two-way distance change. Because LOS measures range change between the satellite and the surface, an increase in LOS reflects surface subsidence, and, vice versa, a decrease in LOS reflects surface uplift.

Spaceborne SAR data have been acquired since the late 1970s by several satellites using various systems and acquisition parameters ([Table 7.1](#)). Two of the key parameters that determine the interaction of the radar signal with vegetation are the radar wavelength (or frequency) and polarization.

TABLE 7.1
Space-Based SAR Sensors

Satellite	Wavelength and Polarization	Agency	Time
SeaSAT	L-band, HH polarization (pol)	DoD	1978
ERS-1	C-band, VV pol	ESA	1992–1996
ERS-2 (SAR)	C-band, VV pol	ESA	1996–2011
JERS-1	L-band, HH pol	JAXA	1992–1998
Radarsat-1	C-band, HH pol	CSA	1995–2013
Space shuttle (SRTM)	X-, C-, and L-band, fixed baseline interferometer	NASA	2000
Envisat (ASAR)	C-band, dual pol	ESA	2002–2012
ALOS (PALSAR)	L-band, dual pol, quad pol	JAXA	2006–2011
Radarsat-2	C-band, quad pol	CSA	2007–present
TerraSAR-X/TanDEM-X	X-band, dual pol, quad pol	DLR	2007–present
COSMO-SkyMed	X-band, dual pol	ASI	2007–present

Source: Wdowinski, S. and Eriksson, S., *EOS Trans. Am. Geophys. Union*, 90, 153, 2009.

Agencies: ASI, Italian Space Agency; CSA, Canadian Space Agency; DLR, German Aerospace Center; DoD, Department of Defense (United States); ESA, European Space Agency; JAXA, Japan Aerospace Exploration Agency; NASA, National Aeronautics and Space Administration (United States).

Most SAR satellites have operated in three frequencies: X-band (wavelength 3.1 cm), C-band (5.6 cm), and L-band (24 cm). It is commonly accepted that the shorter wavelength X-band signal interacts mainly with upper sections of the vegetation, the intermediate C-band signal penetrates further and can penetrate the entire canopy under some circumstances, and the L-band signal can penetrate throughout the vegetation and interact with the surface beneath the vegetation. X-band satellites include the German TerraSAR-X (TSX) and TanDEM-X (TDX) and the Italian COSMO-SkyMed (CSK) constellation. C-band satellites are the ERS-1, ERS-2, and Envisat operated by the European Space Agency and the Radarsat-1 (RSAT-1) and Radarsat-2 (RSAT-2) operated by the Canadian Space Agency. L-band satellites include the Japanese JERS-1 and ALOS-1 satellites, which ceased operation, and the ALOS-2 satellite in which its launch is scheduled for 2014.

Radar polarization determines the direction at which the SAR signal is transmitted from and received at the satellite's antenna. The first generation of SAR satellites operated in a single polarization mode, such as HH (horizontal transmitted and horizontal received) by RSAT-1 or VV (vertical transmitted and vertical received) by ERS-1/2. The second generation of SAR satellites, such as Envisat and ALOS, already operated with dual polarization mode, such as HH+HV (horizontally transmitted and two types of receptions, horizontal and vertical) or VV+VH. RSAT-2 is the only civilian satellite that operates in a full quadruple mode (quad-pol) that acquires data in four independent channels (HH, HV, VH, and VV). ALOS and TSX have been operated in experimental quad-pol modes for short time periods and acquired limited amounts of quad-pol data.

WETLAND InSAR

Wetland InSAR is a unique application of the InSAR technique that detects elevation changes of aquatic surfaces; all other InSAR applications detect displacements of solid surfaces. The technique works, because the radar pulse is backscattered twice ("double bounce") from the water surface and vegetation (Richards et al. 1987; Figure 7.1c). The method was first used with L-band data, which works better in vegetated environments. Alsdorf et al. (2000) analyzed space shuttle L-band data to study water level variations in the Amazon floodplain. Wdowinski et al. (2004, 2008) also used JERS-1 L-band observations of Everglades wetlands for detecting water flow changes throughout



FIGURE 7.3 Photographs of (a) freshwater herbaceous vegetation (saw grasses); (b) mixed vegetation—woody vegetation in the tree island and herbaceous around the islands—(c) freshwater woody vegetation (cypress); and (d) saltwater woody vegetation (mangroves) that grows along a tidal channel.

the wetlands. Although X- and C-band radar signals are often assumed to interact mainly with upper sections of the vegetation, several studies show that both data types are also suitable for the wetland InSAR application (Gondwe et al. 2010; Hong et al. 2010a,b; Lu 2005).

We present the principles, methodology, and results of wetland InSAR using examples from our main study area, the Everglades in south Florida. The Everglades can be viewed as a large-scale laboratory for testing remote sensing hydrological techniques, because it extends over a wide area, consists of a variety of vegetation types (herbaceous, woody, freshwater, and saltwater—Figure 7.3), and contains both controlled and natural hydrological conditions. Furthermore, a dense network of stage gauging stations located throughout the Everglades provides excellent ground truthing data for calibrating and validating the wetland InSAR results. Two sets of interferograms are presented: (1) the freshwater environment, which is dominated by wide and slow sheet flow, and (2) the coastal wetland environment, which is dominated by daily tidal flow. The data were processed using the software package ROI_PAC (Pritchard et al. 2014), which generates interferograms from pairs of the same sensor data.

The freshwater interferograms cover an extensive wetland area located between Lake Okeechobee and the Gulf of Mexico—known as the “River of Grass”—prior to its massive development (Douglas 1947). Today, the area includes the Everglades Agricultural Area (EAA), a series of managed wetlands called Water Conservation Areas (WCAs), and Everglades National Park (ENP) with remnants

of the natural flowing freshwater system (Figure 7.2b). The freshwater interferograms show high variability in the pattern of the detected phase changes, often called fringes, depending on the sensor type and hydrological conditions occurring during the two acquisition times (Figure 7.2). The L-band (24 cm wavelength) ALOS interferograms show that most phase changes occur within a range of a single fringe cycle. Furthermore, some of the fringes are discontinuous (sharp color change) across physical structures, which control hydrology (e.g., levees) reflecting different water level changes across hydrological structures. The C-band interferogram also shows fringe discontinuity across hydrological structures but with a larger number of fringes (Figure 7.2c). The X-band interferogram shows even larger number of fringes, mostly in the WCAs, but some also in the urban area located east of the WCAs. The fringes in the urban area and some in the WCAs reflect changes in the atmospheric precipitable water (moisture) level, which can delay the arrival of the radar signal.

The fringe density and fringe pattern detected in the three interferograms (Figure 7.2b through d) reflect both the sensor's wavelength and the change in water levels between the two acquisition times. As indicated earlier, for a given acquisition geometry (incidence angle), the measured phase change is proportional to the half-wavelength of radar signal. In the example shown in Figure 7.2, one fringe cycle (2π) of L-band signal reflects 15 cm of vertical displacement, 4 cm in C-band interferograms, and 2 cm in X-band. Thus, 12 cm of water level change will be reflected as less than a single L-band fringe cycle (about 0.8 of a cycle), 3 C-band fringes, and 6 X-band fringes. Since SAR satellites acquire their data at a speed of ~ 7 km/s, data acquisition over a 100 km long area takes about ~ 15 s. Consequently, the observed phase change reflects the difference between two acquisition snapshots and not an averaged difference. In some areas, where water level changes occur gradually over long time periods, observed fringes may reflect an average rate of change. But in a dynamic wetland environment, when water levels change frequently due to heavy rain, water management, or ocean tides, InSAR observations measure the difference between the two acquisition snapshots.

Interferograms are color maps displaying phase changes in the range of $0-2\pi$. In order to understand the significance of these maps and their use for calculating water level changes, we zoom into WCA-1 (Figure 7.4). Four interferograms of this area are presented, each with a different fringe pattern and fringe density. The ALOS interferogram (Figure 7.4a) shows variations within one fringe cycle, in which the phase in the interior is higher than along the area's boundaries (according to the scale in Figure 7.2, the range increases from yellow to pink). This phase change pattern of high phase in the interior and lower phase near the boundaries can be easily seen in the phase profile plot across the A-A' transect (second row in Figure 7.4a). The first RSAT-1 interferogram shows a roughly N-S fringe pattern, in which phase increases from west to east (Figure 7.4b). Because the phase change wrapped in the range of $0-2\pi$, the phase change is discontinuous and has a sawtooth shape pattern (second row in Figure 7.4b). The second RSAT-1 interferogram shows a radial fringe pattern, in which phase increases from the area's boundaries toward the interior (Figure 7.4c). In this case, the sawtooth pattern changes from a westward slope (phase increase from west to east) in the western side of the area to an eastward slope in the eastern side (second row in Figure 7.4c). The TSX interferogram shows a combination of radial and linear patterns, which results in a less symmetrical sawtooth pattern (second row in Figure 7.4d).

The discontinuous phase change pattern occurs because the InSAR-detected phase change is wrapped in the range of $0-2\pi$. In order to remove these discontinuities, the phase changes should be unwrapped and expanded over a larger range. The unwrapping procedure is demonstrated in the third row of Figure 7.4, where the phase change pattern is continuous and extends over the range of $0-\pi$ (L-band), $0-14\pi$ (first C-band), $0-7\pi$ (second C-band), and $0-5\pi$ (X-band). All the unwrapped profiles show a phase change decrease from left (west) to right (east) and some increase at the eastern part of the profile. As InSAR calculations correct for a possible change in the SAR satellite positions during the two acquisitions, the observed phase change reflects surface changes with respect to the satellite. A phase change increase indicates surface subsidence, whereas a phase change decrease indicates uplift. The actual amount of subsidence or uplift depends on the sensor's wavelength and the acquisition geometry. For the four interferograms presented in Figure 7.4, one fringe cycle (2π)

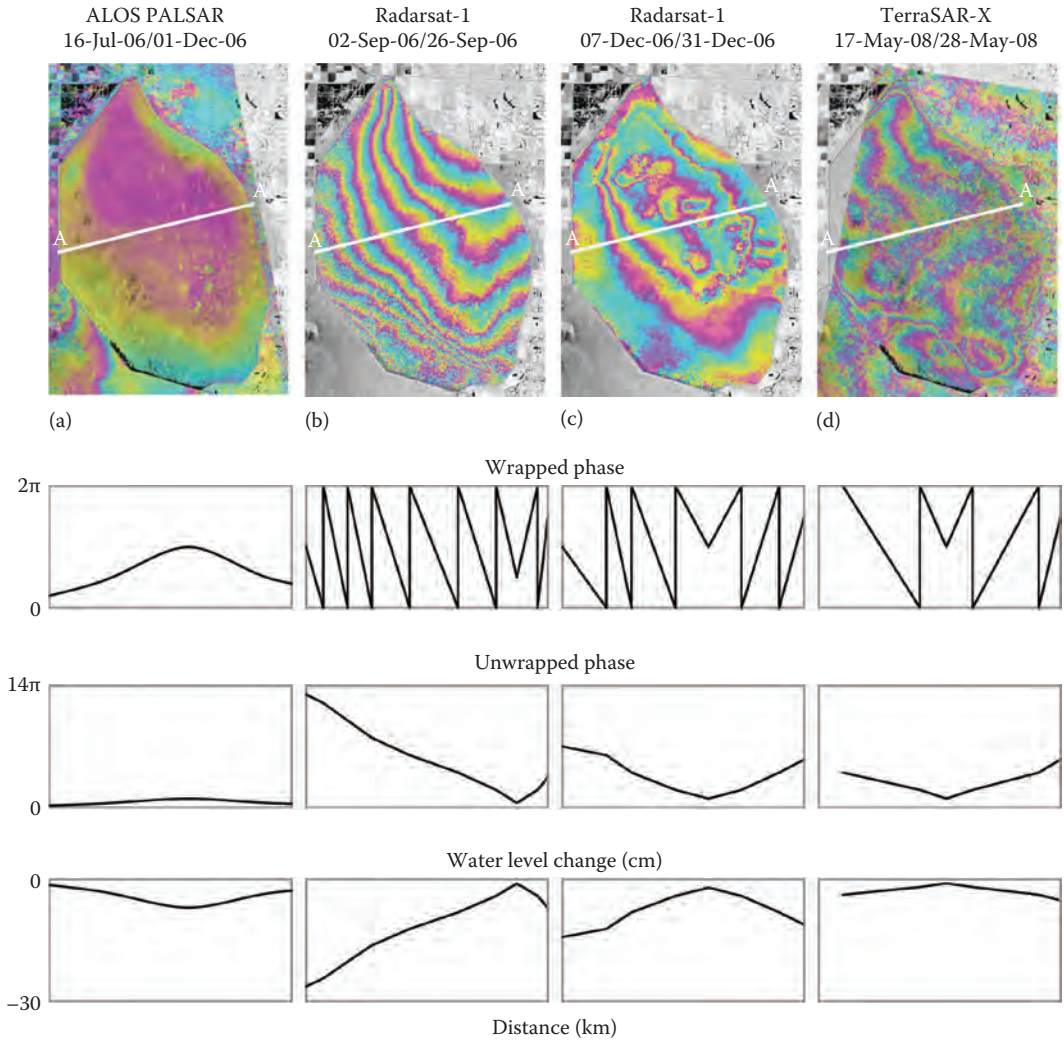


FIGURE 7.4 Phase change and inferred water level changes in WCA-1. Upper row presents ALOS (a), Radarsat-1 (b and c), and TSX (d) interferograms of WCA-1. Second row illustrates phase changes along the A–A’ transect. The phase is wrapped in the range of 0– 2π . The third row illustrates the unwrapped phase, which extends over a larger phase range. The fourth row illustrates the inferred vertical change in water level, which depends on the SAR signal’s wavelength and acquisition geometry.

of the L-, C-, and X-bands corresponds to 15, 4, and 2 cm of vertical surface changes, respectively. The conversion of the phase information to water level changes involves both reversing the fringe shape pattern and multiplication by the sensor’s conversion factor (fourth row in Figure 7.4). In three of the four examples presented in Figure 7.4, the water level change pattern is similar indicating a relative subsidence of the interior part of WCA-1 with respect to the area located near the boundaries. But since InSAR is a relative measurement, the same pattern can also represent a relative uplift of the boundary area with respect to the wetland interior. The water level change pattern in Figure 7.4b shows an overall westward decrease of water levels throughout the area.

The second set of interferograms presented is of coastal wetlands located in the western Everglades (Figure 7.5). The interferograms show a less organized fringe pattern than those in the flow-controlled area (WCAs) (Figure 7.2). The L-band interferogram (Figure 7.5b) shows two

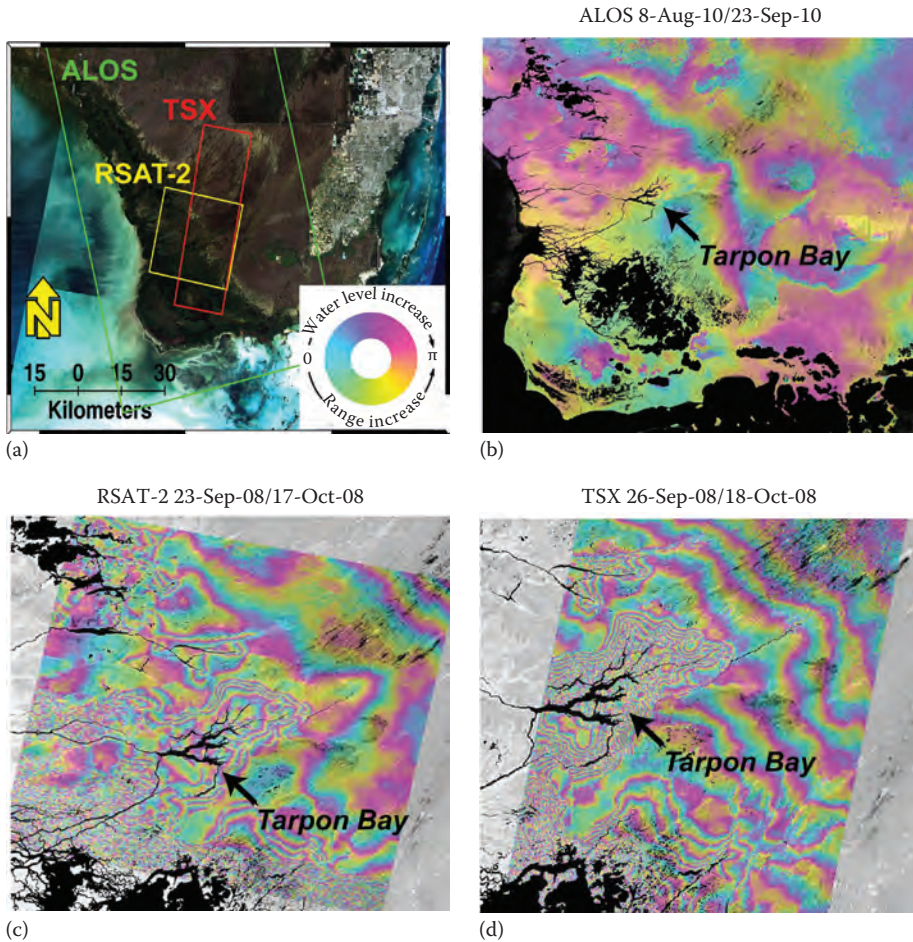


FIGURE 7.5 (a) Google Earth composite satellite image showing the location of the three interferograms used in the coastal wetland area. (b) ALOS interferogram showing a coherent fringe along the transition between fresh- and saltwater vegetation and partial fringe along the tidal channels. (c) Radarsat-2 interferogram showing short wavelength fringes surrounding tidal channels in the mangrove forest area. (d) TerraSAR-X interferogram showing a similar fringe patterns around the tidal channels. The different number of fringes in each interferogram reflects the sensitivity of each sensor to surface changes. Each ALOS (L-band) fringe reflects 15 cm of water level change, Radarsat-2 (C-band) 4 cm, and TerraSAR-X (X-band) 2 cm.

fringes that follow geographic features and most likely reflect water level changes, which are (1) a linear roughly N–S oriented fringe located east of the Tarpon Bay and (2) a rounded fringe surrounding the Tarpon Bay. The location and orientation of the linear fringe follow the transition zone between fresh- and saltwater vegetation reflecting tide-induced water level changes in the salt marshes. The rounded fringe around the Tarpon Bay has a more pronounced appearance in the other interferograms and is discussed in detail in the following.

The RSAT-2 and TSX interferograms show a more complex fringe pattern (Figure 7.5c and d) that can be characterized by the following three zones: low fringe gradient in the northeastern corner, incoherent phase (fuzzy pattern) in the southwest corner, and wide areas in between with high fringe gradient. The low fringe gradient in the northeast corner occurs in the freshwater wetlands. The low gradient reflects slow changes in the freshwater sheet flow and possibly some atmospheric signals. The incoherent signal in the southwest corner occurs over tall mangrove

vegetation, which produces unstable scattering in the C- and X-band SAR signals. The high fringe gradient in the transition zone occurs over variable vegetation types, including intermediate and short mangrove forests.

The fringes that surround Tarpon Bay and other bodies of water reflect water level changes that occur due to the high contrast between fast flow in the channel and slow flow through the saltwater vegetation (Wdowinski et al. 2013). These high fringe gradients mark the extent of the tidal flushing zone, which occurs over a 2–3 km wide area on each side of the tidal channel. Unwrapping the phase changes along the Tarpon Bay in both C- and X-band interferograms indicates a total of 12 cm water level change, about 25% of average daily tidal variation in Tarpon Bay (40–50 cm). It is interesting to note that the InSAR-detected slope (12 cm/2.5 km) is very small, $\sim 5 \times 10^{-5}$, which is less than a 1/100 of a percent. Such a small slope cannot be detected from the ground but can be easily measured by InSAR from space.

CALIBRATION AND VALIDATION

Interferograms provide high-spatial-resolution (10–300 m pixel resolution) maps of surface water level changes over a broad wetland area. In order to utilize these space-based observations for hydrological applications, additional information is needed because the InSAR measurements are relative in both time and space. In time, the measurements provide the change in water level (not the actual water level) that occurred between the data acquisition times. In space, the measurements describe the relative change of water levels in the entire interferogram with respect to a zero change at an arbitrary reference point, because the actual range between the satellite and the surface cannot be determined accurately. However, relative changes between pixels can be determined at the centimeter level. In many other InSAR applications, such as earthquake- or volcano-induced deformation, the reference zero change point is chosen to be in the far field, where changes are known to be negligible (Massonnet et al. 1993). However, in wetland InSAR, the assumption of zero surface change in the far field does not hold, especially in the Everglades, because flow and water levels can be discontinuous across the various water-control structures or other flow obstacles.

In order to utilize the high-spatial-resolution InSAR observations, independent observations of water levels can be used for calibrating and validating the InSAR observations. The simplest calibration method relies on ground-based stage data as introduced by Wdowinski et al. (2004, 2008). When stage data are not available, calibration can be conducted using space-based altimetry data that were acquired during the same time span as the InSAR data (Kim et al. 2009). Here, we briefly describe the stage-based calibration technique using an example of an RSAT-1 interferogram from south Florida (Figure 7.6a) and stage data that are available at the SFWMD's DBHYDRO database (SFWMD 2014; for more details of the calibration method, see Wdowinski et al. 2008).

The stage-based calibration procedure involves the following four steps: phase unwrapping, stage data retrieval, InSAR–stage data comparison, and InSAR data adjustment. The first step is phase unwrapping for calculating the InSAR-determined water level changes with respect to an arbitrary reference point that is set with a value of zero. The phase unwrapping is conducted independently for each body of water (WCA-1, 2A, 2B, 3A, 3B, ENP), as water level changes can be discontinuous across barriers (e.g., levees). For each stage station location (Figure 7.6c), the InSAR-derived water level change is calculated by averaging values from nine pixels surrounding the station location. In parallel (step two), the stage-derived value is calculated by subtracting the stage record from the two acquisition dates. The comparison between the InSAR- and stage-derived water level changes (step three) is conducted separately for each body of water, as shown in Figure 7.6b. In all areas, the data are fitted using a straight line with a slope of one ($y=x+b$), in order to determine the y-axis intercept value, which is used to calibrate the InSAR data. In the final step, we subtract the intercept value from the InSAR water level change observation, so they best fit the stage-derived levels. In some areas, such as WCA1, the fit between the two independent datasets is very good, whereas in

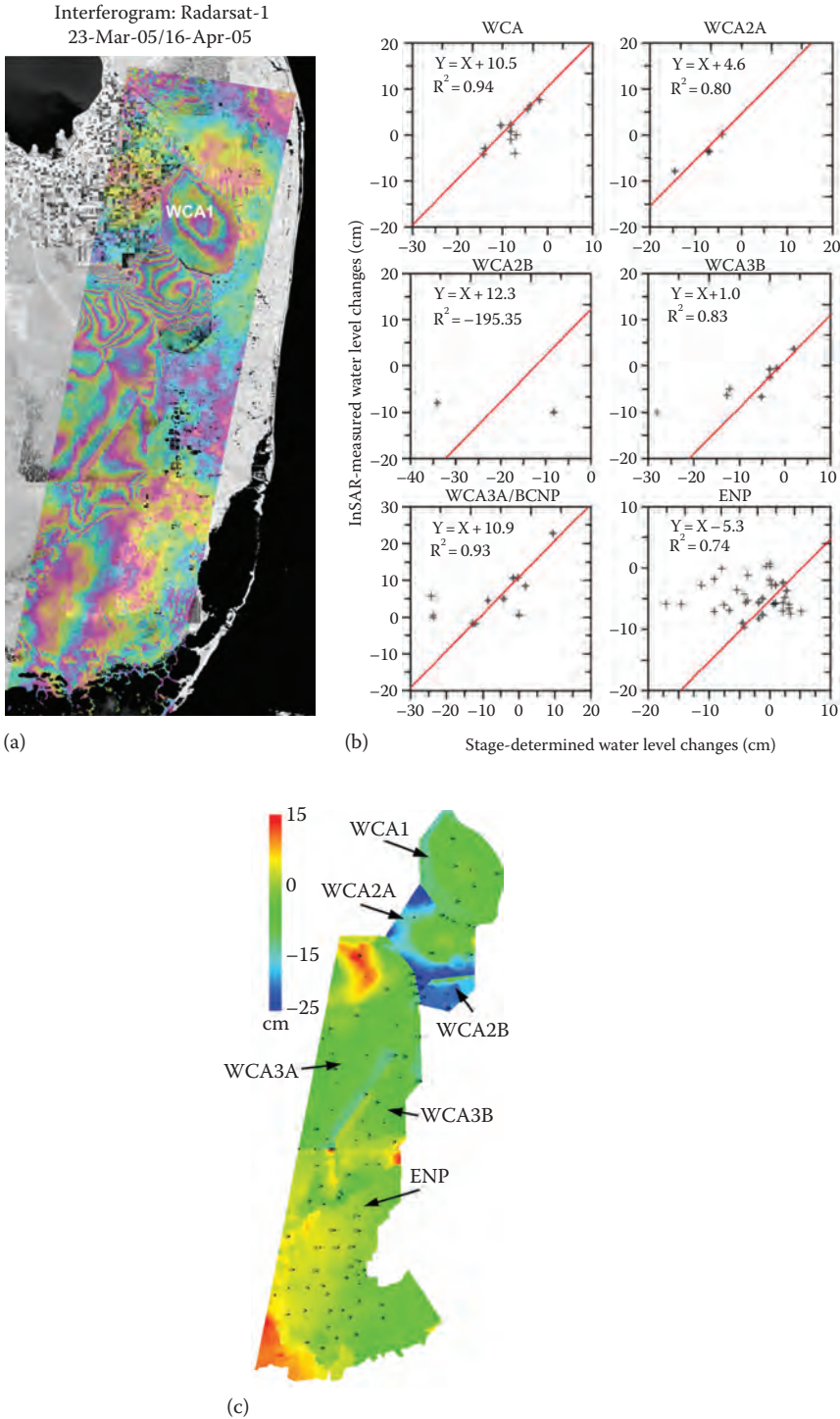


FIGURE 7.6 (a) Radarsat-1 interferogram showing phase changes in response to changes in water levels that occurred between the two acquisition dates. (b) InSAR–stage calibration plots for each water body. The water bodies and stage station locations are shown in Figure 7.5c. (c) InSAR-derived map of water level changes that occurred between March 23, 2005, and April 16, 2005. The black dots mark the location of the stage stations.

others (e.g., ENP) is not. The poor fit in the ENP most likely reflects water level decreases below the surface, which are still measured by the gauging stations, but invisible to InSAR measurements.

The quantitative comparison between InSAR and stage data allows us to determine the accuracy of the InSAR technique. We found accuracy of the L-band data in the range of 3–5 cm (Hong and Wdowinski 2014; Wdowinski et al. 2008), whereas the accuracy of C-band RSAT-1 data was slightly worse, in the range of 6–7 cm (Hong et al. 2010b). These low accuracy levels most likely reflect low interferometric coherence (see next section), close proximity of some stage gauging stations to hydrological structures, and atmospheric noise.

INTERFEROMETRIC COHERENCE OF WETLANDS

Interferometric coherence is a quality measure of an interferogram, which calculates spatial consistency of the calculated phase. High interferometric coherence is reflected in continuous fringe patterns, whereas low coherence appears as a fuzzy phase pattern (e.g., lower part of Figure 7.5c). We use coherence maps to evaluate which data type and acquisition parameters are most suitable for the wetland application of InSAR. As coherence strongly depends on the vegetation type, we used the diverse Everglades vegetation to evaluate coherence values over the various vegetation types. We subdivided the study area into the following five wetland vegetation types: freshwater woody vegetation (cypress), saltwater woody vegetation (mangroves), freshwater herbaceous vegetation (saw grass), freshwater grassy vegetation (graminoid), and mixed vegetation (mixed shrubs) (Figure 7.7a). Some of these vegetation types can be seen in Figure 7.3. Our study includes the analysis of C- and L-band SAR data that were acquired by the ERS-1/2, RSAT-1, Envisat, and JERS-1 satellites.

A robust coherence analysis of the various data types and vegetation types was conducted by Kim et al. (2013). Here, we present a brief summary of the coherence analysis. Our results indicate that woody wetlands like cypress and mixed shrubs marsh have better coherence than herbaceous wetlands like saw grass and cattail in all satellite systems (Figure 7.7c). The L-band JERS InSAR pairs, as much as 3 years apart, still maintained adequate coherence in wetlands, especially in woody wetlands, while C-band ERS-1/2 required short temporal baselines (<70-day) to maintain coherence in herbaceous wetland. Our study also clearly indicates that HH polarization with high resolution and small incidence angles is more suitable to wetland InSAR application in terms of decorrelation. Further details of the coherence analysis and explanations for the results are provided by Kim et al. (2013).

INSAR TIME SERIES

A significant progress in InSAR technology was the development of permanent scatterer InSAR (PS-InSAR) (Ferretti et al. 2000, 2001) and small baseline subset (SBAS) techniques (Berardino et al. 2002; Lanari et al. 2004), which use a large number of SAR observations to monitor time series of displacement using successive InSAR observations. These techniques are very useful for monitoring slow and continuous deformation of the Earth's solid surface mainly in urban areas. However, these methods do not work in the rapidly changing wetland or floodplain environments, which are subjected to rapid water level changes. Thus, we developed a new technique—small temporal baseline subset (STBAS)—which utilizes highly coherent interferometric phases obtained only with relatively short time difference between two SAR acquisitions of a single satellite track (Hong et al. 2010b). The STBAS technique integrates InSAR and stage observations to transform relative wetland InSAR observations to absolute frame and generates both detailed maps of water levels and water level time series for almost each pixel (40 m resolution). We successfully applied the STBAS technique to WCA-1 by using RSAT-1 and stage data spanning over a 2-year period (2006–2008) and obtained a time series of high-spatial-resolution water level maps, almost every 24 days, which is the RSAT-1 satellite repeat pass period.

In order to increase the observation frequency, we recently expanded our method to incorporate water level maps calculated from several tracks. Although the observation frequency in each track

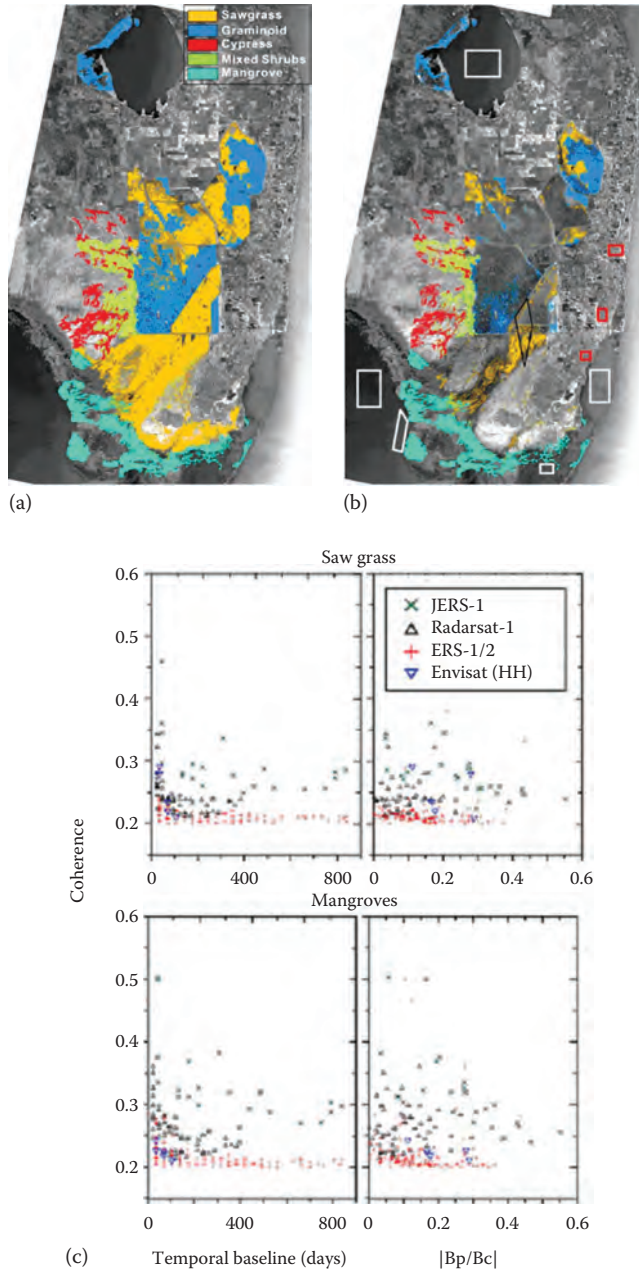


FIGURE 7.7 Characteristic wetland environments in the Everglades superimposed on ERS multifrequency SAR image. (a) Selected five wetland types based on 1999 land cover map distributed from SFWMD (South Florida Water Management District) and NLCD (National Land Cover Database) 2001 land cover map. (b) Five typical marshes with low backscattering variation selected for statistical analysis of coherence and backscatter using ERS-1/2, JERS-1, and Radarsat-1 backscatter variation map. White polygons and red polygons indicate open water surface and urban area, respectively. Backscatter and coherence are used to estimate background noisy coherence and evaluate radar backscatter calibration accuracy. Black polygon represents saw grass marsh covered by all of four different Radarsat-1 observations. (c) Comparison between the coherence obtained with the JERS-1, Radarsat-1, ERS, and Envisat SAR data as a function of time interval between acquisitions and baseline normalized by the critical baseline of each SAR system.

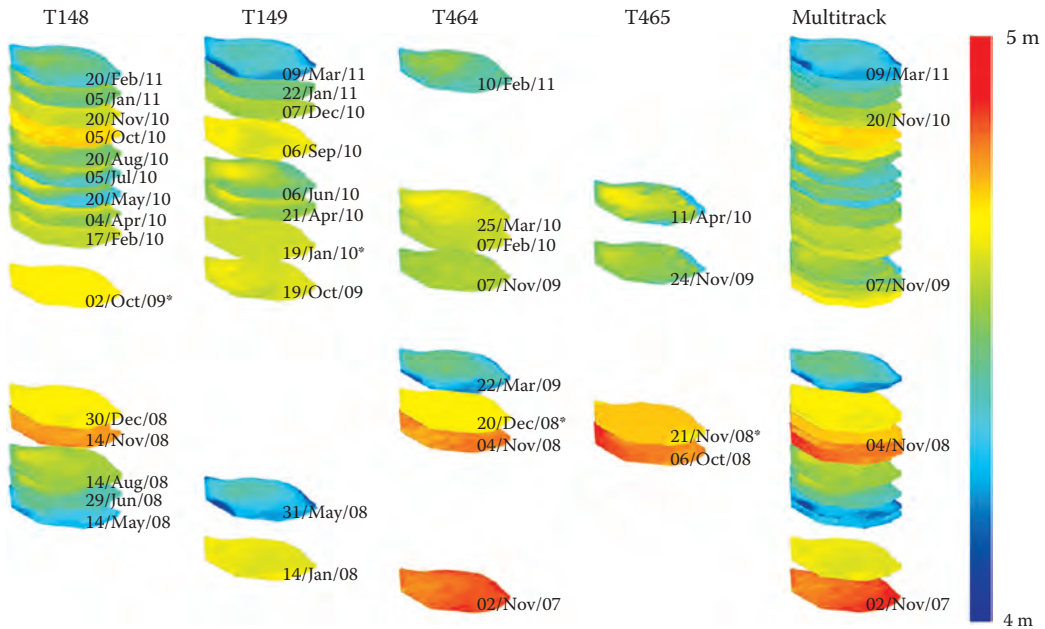


FIGURE 7.8 InSAR-derived high-spatial-resolution water level map time series of WCA-1. The four left columns present the results of four single-track time series analyses, and the right column presents the combined multitrack results. The time span between maps in the single-track solutions is 46 days and its multiples. The time span between maps in the multitrack solution varies between 7 and 194 days, depending on data availability.

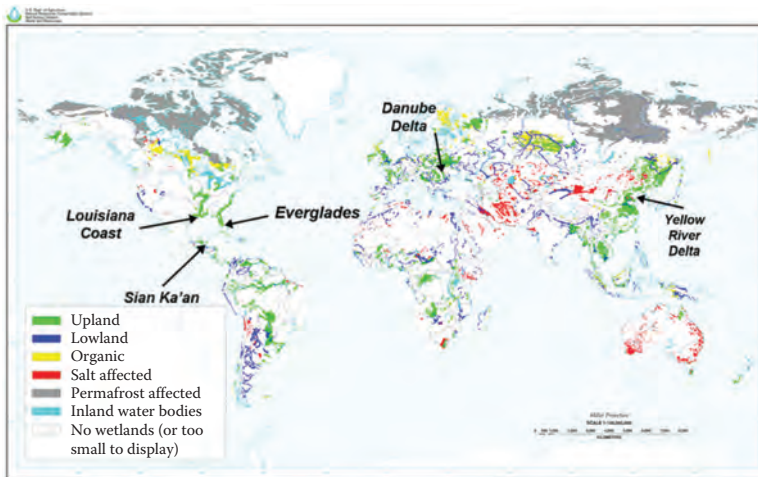
depends on the satellite's repeat pass, the multitrack algorithm can increase the observation frequency to a third or a quarter of the repeat pass orbit, depending on the data availability. Although we cannot process InSAR data from different tracks, we can combine the results from the different tracks as all water level maps are calibrated with the same set of stage data and are tied to the stage stations' datum. We applied the multitrack algorithm again to WCA-1 using ALOS PALSAR data acquired along four tracks during 2007–2011 and stage data (Figure 7.8). Our results indicate a significant increase in the observation frequency from 46 days, which is ALOS' repeat pass period, up to 7 days in the best case.

WETLAND IN SAR STUDIES OF VARIOUS WETLAND ENVIRONMENTS

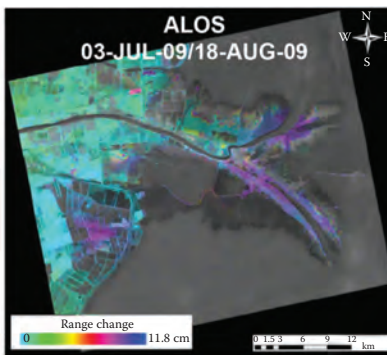
So far, we presented wetland InSAR results from our main study area, the south Florida Everglades. Here, we expand the geographic location and present wetland InSAR observations from other wetland areas around the globe (Figure 7.9). The results of four studies are presented—all showing the successful application of the wetland InSAR technique to monitor remotely water level change and better understand the hydrological regime of the subject wetlands.

YELLOW RIVER DELTA WETLANDS

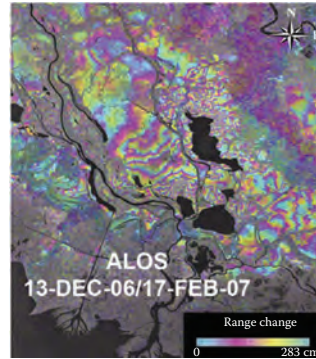
The Yellow River Delta is located in eastern China, where the river meets the Bohai Sea. The delta is a dynamic landform changing locations and patterns due to the large sediment supply. The delta contains a large area of coastal wetlands, including tidal flats, reed marshes, swamp forests, and saline marshes (Xiea et al. 2013). Wetland InSAR analysis of L-band ALOS data acquired during



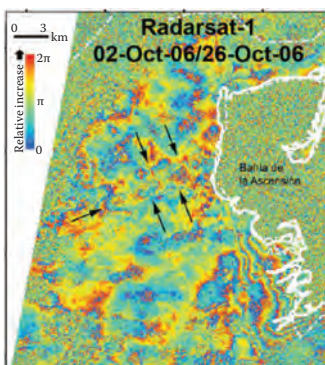
(a)



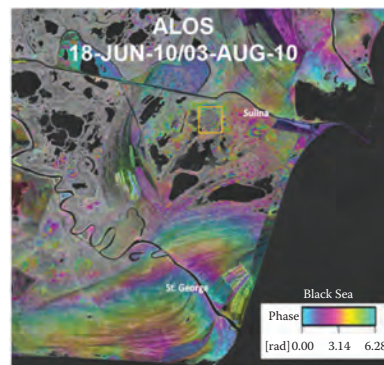
(b)



(c)



(d)



(e)

FIGURE 7.9 (a) Global distribution of wetlands. (From <http://www.nrcs.usda.gov/wps/portal/nrcs/detail/soils/use/worldsoils>.) (b) ALOS interferogram of the Yellow River Delta in China. (From Xiea, C. et al., *Int. J. Remote Sens.*, 34, 2047, 2013.) (c) ALOS interferogram of woody wetlands along the Louisiana Coast in the United States. (From Kim, J.W. et al., *Remote Sens. Environ.*, 113, 2356, 2009.) (d) Radarsat-1 interferogram of the Sian Ka'an (Yucatan, Mexico) wetlands. (From Gondwe, B.R.N. et al., *Wetlands*, 30, 1, 2010.) (e) ALOS interferogram of the Danube Delta (Romania). (From Poncos, V. et al., *J. Hydrol.*, 482, 79, 2013.)

the years 2008–2009 indicates a good interferometric coherence over the reed marsh vegetation and some of the tidal flats (Figure 7.9b). Combined analysis of the InSAR and ground-based water level observations suggests that most of the InSAR-observed water level changes occurred due to tidal variations, especially in the tidal flats (Xiea et al. 2013).

LOUISIANA WETLANDS

Southern Louisiana is rich in both coastal and inland wetlands, as excess water from the Mississippi River drainage gateway accumulates on the region's very flat topography. The coastal wetlands, built on deltaic plains, are shrinking at a fast rate due to the combined effect of (1) sea level rise, (2) rapid subsidence, and (3) limited sediment supply due to the construction of flood prevention levees along the main rivers. The inland wetlands were also affected by the construction of these levees but since have stabilized. Both coastal and inland wetlands contain diverse habitats from forested swamps to marshes and floating mats. Wetland InSAR was successfully applied to examine water level changes in several wetland environments located in southern Louisiana (Kim et al. 2009; Lu 2005; Lu and Kwoun 2008). Interferometric analysis of ERS-1/2, RSAT-1, and ALOS data revealed that best results were obtained when using L-band data with HH polarization (ALOS). C-band data with HH polarization also revealed reasonable results especially with short time span interferograms. All observation types showed higher coherence over forested swamps and patchy fringe patterns, reflecting flow discontinuities due to man-made and natural barriers (Figure 7.9c).

SIAN KA'AN BIOSPHERE RESERVE

The Sian Ka'an wetlands are located along the east coast of the Yucatan Peninsula, Mexico. The pristine wetlands are fed by groundwater from the karst aquifer of the peninsula. Because most of the inflow occurs through underground karst structures, it is difficult to observe and understand the wetland hydrology. Gondwe et al. (2010) used RSAT-1 observations acquired between July 2006 and March 2008 to detect water level changes in the wetlands and infer the dynamic nature of the system. Their study revealed large variation in the flooded area, in which the main water input areas are associated with water-filled faults that transport groundwater from the catchment to the wetlands. The wetland InSAR observations also revealed local-scale water divides and surface water flow directions within the wetlands (Figure 7.9d).

DANUBE DELTA WETLANDS

The Danube Delta is located at the outlet of the Danube River to the Black Sea, mostly in Romania. The delta's hydrology is dominated by a network of tributaries that supply water and nutrients to a variety of aquatic ecosystems, including lakes, ponds, and marshes. Poncos et al. (2013) used ALOS data from the years 2007–2010 to detect water level changes in the delta (Figure 7.9e). They combined the InSAR observations with stage measurements and hydrological modeling to characterize the surface flow in the marshes and tributaries. Their study revealed a very dynamic flow regime in which the flow direction in the marshes varies frequently depending on the water supply from the tributaries.

DISCUSSION

The unique wetland application of the InSAR technique provides high-spatial-resolution observations (1–50 m pixel resolution) that cannot be obtained by any terrestrial technique. However, the main disadvantage of the wetland InSAR observations is their relative nature. The observations are relative in both space (with respect to a reference point) and time (water level changes between

two acquisition times). Thus, it is important to tie the space-based observations to ground observations of water levels (stage monitoring). In the Everglades, there is a dense stage network, which allows us to calibrate and validate the InSAR observations and tie them to an absolute reference frame. Our calibration studies suggest an accuracy level of 3–8 cm (Hong and Wdowinski 2014; Wdowinski et al. 2004, 2008). The man-made structures in the Everglades create many flow discontinuities that require such dense network for accurate and reliable monitoring. However, in natural flow wetland areas, such as in the ENP in the southern part of the Everglades ecosystem, the flow is continuous and can be monitored by a less dense network. Thus, sparsely distributed stage stations in natural wetland areas may be sufficient for calibrating the InSAR observations. In remote wetland areas, where no stage monitoring exists, one can use altimetry data for InSAR calibration, as used by Kim et al. (2009). However, altimeter observations are also characterized by low temporal resolution and may acquire at a different time than the SAR acquisitions. Nevertheless, altimeter observations can be useful for calibration, if no other accurate measurements can be obtained.

One very useful and important observation can be derived directly from the raw interferogram, without the need of stage data for calibration. The high-resolution wetland interferograms provide direct observations of flow patterns and flow discontinuities, as shown in [Figure 7.2](#). As water level and water level changes tend to be different across barriers, these differences will be shown in the interferogram as phase discontinuities. This observation is important for wetland restoration efforts that aim to restore managed or degraded wetlands, such as the Everglades, to their natural undisturbed condition.

Another very important application of wetland InSAR is constraining high-resolution flow models, which are important tools for wetland management and restoration. This application also does not require stage calibration, as the model results can be converted into the interferogram phase domain. The stage data are typically used as boundary conditions of the flow model. We conducted such preliminary study by comparing the InSAR observations with the TIME (Tides and Inflows in the Marshes of the Everglades) model, which was developed by U.S. Geological Survey and University of Miami. Our study indicates that the model predicts longer-wavelength water levels well, which are constrained by the stage data, but misses many of the shorter-wavelength features.

CONCLUSION

The unique wetland application of the wetland InSAR technique provides high-spatial-resolution observations of surface water level changes in aquatic environments with emergent vegetation, such as wetlands and floodplains. The technique works because of the “double-bounce” effect, in which the radar pulse is backscattered twice, first from the water surface and then from the vegetation, or vice versa. Interferometric coherence analysis of various SAR data types indicates that longer wavelength (L-band), short revisit cycles, HH polarization, high spatial resolution, and small incidence angle are more suitable to wetland InSAR application in terms of decorrelation. Best results have been obtained with the L-band (ALOS and JERS-1) data, X-band (TSX) data with 11-day repeat orbits, and fine beam (7 m resolution) C-band RSAT-1/2 data with 24-day repeat orbits. The application of the wetland InSAR technique to various wetland environments around the world shows that in many wetland areas, interferometric coherence can be maintained and, furthermore, the wetland InSAR observations can provide high-spatial-resolution observations that cannot be obtained by any terrestrial technique. In addition to high-spatial-resolution water level monitoring, wetland InSAR applications include detection of flow patterns and flow discontinuities and constraining high-resolution flow models. The development of the wetland InSAR time series techniques (Hong and Wdowinski 2014; Hong et al. 2010b) provides improved high-spatial, multitemporal water level observations that can be helpful for water management and hydrological modeling.

ACKNOWLEDGMENTS

This work was enabled by the TSX science proposal (HYD0029) and the SOAR project from CSA for access to the TerraSAR-X and the Radarsat-1/2 data. We also thank JAXA and ASF for access to ALOS data. The research was supported by NASA Cooperative Agreement No. NNX10AQ13A (WaterSCAPES: Science of Coupled Aquatic Processes in Ecosystems from Space) and by the National Science Foundation through the Florida Coastal Everglades Long-Term Ecological Research program under Grant No. DEB-1237517.

REFERENCES

- Alsdorf, D.E., J.M. Melack, T. Dunne, L.A.K. Mertes, L.L. Hess, and L.C. Smith. 2000. Interferometric radar measurements of water level changes on the Amazon flood plain. *Nature* 404:174–177.
- Berardino, P., G. Fornaro, R. Lanari, and E. Sansosti. 2002. A new algorithm for surface deformation monitoring based on small baseline differential SAR interferograms. *IEEE Transactions on Geoscience and Remote Sensing* 40:2375–2383.
- Douglas, M.S. 1947. *The Everglades: River of Grass*. Rinehart and Company, New York.
- Evans, T.L. and M. Costa. 2013. Landcover classification of the Lower Nhecolandia subregion of the Brazilian Pantanal Wetlands using ALOS/PALSAR, RADARSAT-2 and ENVISAT/ASAR imagery. *Remote Sensing of the Environment* 128:118–137.
- Ferretti, A., C. Prati, and F. Rocca. 2000. Nonlinear subsidence rate estimation using permanent scatterers in differential SAR interferometry. *IEEE Transactions on Geoscience and Remote Sensing* 38:2202–2212.
- Ferretti, A., C. Prati, and F. Rocca. 2001. Permanent scatterers in SAR interferometry. *IEEE Transactions on Geoscience and Remote Sensing* 39:8–20.
- Gondwe, B.R.N., S.H. Hong, S. Wdowinski, and P. Bauer-Gottwein. 2010. Hydrologic dynamics of the ground-water-dependent Sian Ka'an Wetlands, Mexico, derived from InSAR and SAR data. *Wetlands* 30:1–13.
- Hong, S.H. and S. Wdowinski. 2014. Multi-temporal, multi-track monitoring of wetland water levels in the Florida Everglades using ALOS PALSAR data with interferometric processing. *Geoscience and Remote Sensing Letters* 11:1355–1359.
- Hong, S.H., S. Wdowinski, and S.W. Kim. 2010a. Evaluation of TerraSAR-X observations for wetland InSAR application. *IEEE Transactions on Geoscience and Remote Sensing* 48:864–873.
- Hong, S.H., S. Wdowinski, S.W. Kim, and J.S. Won. 2010b. Multi-temporal monitoring of wetland water levels in the Florida Everglades using interferometric synthetic aperture radar (InSAR). *Remote Sensing of the Environment* 114:2436–2447.
- Kim, J.W., Z. Lu, H. Lee, C.K. Shum, C.M. Swarzenski, T.W. Doyle, and S.H. Baek. 2009. Integrated analysis of PALSAR/Radarsat-1 InSAR and ENVISAT altimeter data for mapping of absolute water level changes in Louisiana wetlands. *Remote Sensing of the Environment* 113:2356–2365.
- Kim, S.W., S. Wdowinski, A. Amelung, T.H. Dixon, and J.S. Won. 2013. Interferometric coherence analysis of the Everglades wetlands, South Florida. *IEEE Transactions on Geoscience and Remote Sensing* 51:1–15.
- Kwoun, O.I. and Z. Lu. 2009. Multi-temporal RADARSAT-1 and ERS backscattering signatures of coastal wetlands in southeastern Louisiana. *Photogrammetric Engineering and Remote Sensing* 75:607–617.
- Lanari, R., O. Mora, M. Manunta, J.J. Mallorqui, P. Berardino, and E. Sansosti. 2004. A small-baseline approach for investigating deformations on full-resolution differential SAR interferograms. *IEEE Transactions on Geoscience and Remote Sensing* 42:1377–1386.
- Lu, Z. 2005. C-band radar observes water level change in swamp forests. *EOS, Transactions, American Geophysical Union* 86:141–144.
- Lu, Z. and O.I. Kwoun. 2008. Radarsat-1 and ERS InSAR analysis over southeastern coastal Louisiana: Implications for mapping water-level changes beneath swamp forests. *IEEE Transactions on Geoscience and Remote Sensing* 46:2167–2184.
- Massonnet, D., M. Rossi, C. Carmona, F. Adragna, G. Peltzer, K. Feigl, and T. Rabaute. 1993. The displacement field of the Landers earthquake mapped by radar interferometry. *Nature* 364:138–142.
- Poncos, V., D. Teleaga, C. Bondar, and G. Oaie. 2013. A new insight on the water level dynamics of the Danube Delta using a high spatial density of SAR measurements. *Journal of Hydrology* 482:79–91.
- Pritchard, M.E. and Contributors to the ROI_PAC wiki. Version: 0.4. 2014. Open-source software for geodetic imaging: ROI_PAC for InSAR and pixel tracking. Available online at: http://www.geo.cornell.edu/eas/PeoplePlaces/Faculty/matt/pub/winsar/InSAR_textbook_for_web_2014.pdf.

- Richards, L.A., P.W. Woodgate, and A.K. Skidmore. 1987. An explanation of enhanced radar backscattering from flooded forests. *International Journal of Remote Sensing* 8:1093.
- SFWMD. 2014. DBHYDRO—Corporate environmental database. Available online at: <http://www.sfwmd.gov/dbhydro>. <http://www.sfwmd.gov/org/ema/dbhydro/index.html>.
- Simard, M., K.Q. Zhang, V.H. Rivera-Monroy, M.S. Ross, P.L. Ruiz, E. Castaneda-Moya, R.R. Twilley, and E. Rodriguez. 2006. Mapping height and biomass of mangrove forests in Everglades National Park with SRTM elevation data. *Photogrammetric Engineering and Remote Sensing* 72:299–311.
- Wdowinski, S., F. Amelung, F. Miralles-Wilhelm, T.H. Dixon, and R. Carande. 2004. Space-based measurements of sheet-flow characteristics in the Everglades wetland, Florida. *Geophysical Research Letters* 31:L15503.
- Wdowinski, S. and S. Eriksson. 2009. Geodesy in the 21st century. *EOS, Transactions American Geophysical Union* 90:153–155.
- Wdowinski, S., S.-H. Hong, A. Mulcan, and B. Brisco. 2013. Remote-sensing monitoring of tide propagation through coastal wetlands. *Oceanography* 26(3):64–69, DOI 10.5670/oceanog.2013.46.
- Wdowinski, S., S.W. Kim, F. Amelung, T.H. Dixon, F. Miralles-Wilhelm, and R. Sonenshein. 2008. Space-based detection of wetlands' surface water level changes from L-band SAR interferometry. *Remote Sensing of the Environment* 112:681–696.
- Xie, C., Y. Shao, J. Xue, Z. Wang, and L. Fanga. 2013. Analysis of ALOS PALSAR InSAR data for mapping water level changes in Yellow River Delta wetlands. *International Journal of Remote Sensing* 34:2047–2056.